Nanomed Res J 8(1): 24-36, Winter 2023

RESEARCH ARTICLE

Cardioprotective role of biosynthesized gold nanoparticles compared to an iodinated-based x-ray contrast agent in Male Wistar Rats

Paul Sola Ayanlola [1,*], Gbadebo Adebisi Isola [1], Waidi Adeoye Saka[2,*], Margaret Kofoworola Akinloye[1], Yekinni Kolawole Sanusi[1], Oluwaseun Adedokun[1], Mustapha Kola Lawal[3], Gabriel Alamu Alamu[1] and Esther A. Adeoje[1]

[1] Department of Pure and Applied Physics, Faculty of Pure and Applied Sciences, Ladoke Akintola University of Technology, Ogbomoso, Nigeria.
[2] Department of Physiology, Faculty of Basic Medical Sciences, Ladoke Akintola University of Technology, Ogbomoso, Nigeria.
[3] Department of Science Laboratory Technology, Faculty of Pure and Applied Sciences, Ladoke Akintola University of Technology, Ogbomoso, Nigeria.

ARTICLE INFO

Article History:
Received 26 Dec 2022
Accepted 22 Jan 2023
Published 15 Feb 2023

Keywords:
Cardioprotective
Biosynthesize
Gold nanoparticles
Contrast agent
Biomedical applications

ABSTRACT

Contrast agents (CAs) are used in medical imaging to enhance the visibility of radiographic images. However, its circulation affects the hemodynamics of the cardiovascular system through which the substance traverses. With the advent of nanotechnology, gold nanoparticles (AuNPs) have been proposed as a potential CA to overcome the limitations of the existing one, but the challenges encountered in the physical and chemical methods of synthesizing AuNPs have resulted in studies suggesting biological methods. This research, therefore, synthesized and characterized AuNPs using the extract of *Psidium guajava* and *Corchorus olitorius* and compared their performance with an existing CA (ECA) administered to rats and irradiated at 40, 80, and 120 kV of x-ray respectively, at an exposure current of 8 mAs on cardiac functions. The morphology of the particles is spherical, with an average size of 8.23 ± 1.03 nm for the AuNPs capped with *P. guajava* and 6.57 ± 1.62 nm for the AuNPs *capped* with *C. olitorius.* The results obtained for the biomarkers revealed that the group injected with the ECA showed a significant decrease in antioxidants with a concomitant increase in cardiac and inflammatory markers at $p < 0.05$ compared to those of the control and those injected with the synthesized AuNPs. The photomicrograph revealed a little difference in the cellular structure for the group of rats injected with the ECA compared to those injected with the synthesized AuNPs. Hence, this study has established that green synthesized AuNPs can be applied for several biomedical applications without posing any threat to the hearts.

How to cite this article
Ayanlola P. S., Isola G. A., Saka W. A., Akinloye M. K., Sanusi Y. K., Adedokun O., Lawal M. K., Alamu G. A., Adeoje E. A., Cardioprotective role of biosynthesized gold nanoparticles compared to an iodinated-based x-ray contrast agent in Male Wistar Rats. Nanomed Res J, 2023; 8(1): 24-36. DOI: 10.22034/nmrj.2023.01.003

INTRODUCTION

As clinical experiences broaden human knowledge, changes in diagnosis and treatment are required, thus imaging is employed to accurately diagnose health problems [1, 2]. However, the similarity in the physical characteristics of some anatomical features may make those features not to be distinguished radiographically from their surrounding tissues. Hence, to assist medical practitioners in efficiently visualizing abnormality and to achieve high-resolute images, contrast agents (CAs) are used in different x-ray imaging modalities, with the existing CA (ECA) based on iodine and barium molecules [1 - 4].

Upon administration, the distribution of CA is regulated by the cardiovascular system [5], however, its circulation may affect and perturb the hemodynamic of the cardiovascular system

* Corresponding Author Email: *wsaka@lautech.edu.ng; psay-anlola28@lautech.edu.ng*

[6] and other associated organs through which the substance traverses. An action that may be followed by destruction in free radicals, upsurge in the activity of cardiac indicators, and pro-inflammatory cytokines [7], as well as oxidative stress, calcium overload, injury to the myocardial and endothelial cells, contractile dysfunction, necrosis, and/or apoptosis-induced cell death [8]. Hence, cardiovascular disease (CVD) is the leading cause of death worldwide, claiming about 17.9 million lives a year [9] and this is a major cause of concern regarding the use of CA. More so, reports from previous studies have it that, over the last three decades, there has been no fundamental improvement in the currently used CAs [10], despite their limitations in medical imaging [11].

With the incorporation of nanomaterials into medicine, several progresses have been made in the development of materials and devices suitable for medical applications. Of utmost interest in this study is the call for the use of nanoparticles (NPs) as CAs in x-ray imaging to overcome the limitations of the ECAs [11, 12]. One of the NPs that has gained significant attention as a promising CA is gold nanoparticles (AuNPs). This is because AuNPs is very easy to synthesize, its properties can be controlled, high attenuation coefficient at the diagnostic energy level, and biocompatibility. Gold (Au) has a high atomic number (Z = 79) compared to iodine (Z = 53) and barium (Z = 56) and thus absorbs more x-rays at specific energy levels [13]. Various methods of synthesizing AuNPs are documented in the literature in terms of control over size, morphology, and surface chemistry, most of which involve the use of physical or chemical methods. However, the use of expensive technologies and non-biocompatibility challenges associated with the physical and chemical methods have resulted in studies suggesting the use of biological methods [14].

The biological method involves the use of microorganisms and plants, with plants and plant materials having a superior advantage over other biological processes. This is because synthesizing NPs from plants eliminates the process of maintaining microorganisms, the process do not need multi-step procedures [15, 16], and can be easily scaled up for large-scale production [17]. In addition, the abundance of several phytochemicals and antioxidants present in *Psidium guajava* (guava)) and *Corchorus Olitorius (*Jute mallow) have been found to be beneficial medically [18, 19]. Other studies have also demonstrated that these plants exhibit anti-cancer, anti-inflammatory, and anti-proliferative activities in various *in-vitro* and *in-vivo* evaluations [18 - 20].

This study, therefore, synthesize AuNPs using the extract of *P. guajava* and *C. olitorius* and their properties were determined using different spectroscopy and microscopy techniques. The performance of an existing iodine-based CA and the synthesized AuNPs were thereafter evaluated on cardiac biomarkers of rats exposed to different tube voltage of x-rays. The novelty of the study lies in the use of orthodox plants (*P. guajava* and *C. olitorius)* that are readily available, cheap, and of high medicinal value in synthesizing AuNPs for use as a contrast agent, in order to disperse the fear arising from the cellular toxicity, mutagenicity, or genotoxic effects of chemically prepared AuNPs in medical imaging applications. The synthesis of AuNPs using plant extract has been reported for different biological applications such as cardioprotective [21], antiparasitic [22, 23], antioxidant [24, 25], anticancer activities [26 - 29], antibacterial [25, 30] and many more. However, to the best of our findings, this is the first study comparing the cardioprotective role of biosynthesized AuNPs and an existing iodinated CA.

MATERIALS AND METHODS

The procedure followed in conducting the experiment are as shown in Fig. 1.

Preparation of extracts

Leaves of *P. guajava* and *C. Olitorius* were obtained from the Teaching and Research Farm of Ladoke Akintola University of Technology, Ogbomoso. The collected plant samples were rinsed with distilled water, air dry, pulverized, and passed through a 2 mm mesh. 10 g of each powdery sample was dissolved in 200 ml of 70% ethanol solution and stirred for 5 mins, the mixture was thereafter sealed with aluminium foil and heated for 5 min at 50˚C to aid the formation of aqueous extract. The resulting solution was allowed to cool for 24 h and then filtered through Whatman No. 1 filter paper, and stored in a cleaned bottle pending further usage.

Synthesis

1 mL of each prepared extract was added to 20 mL 1 mM $HAuCl_4$ (prepared from the stock salt of tetrachloroauric (III) acid trihydrate ($HAuCl_4.3H_2O$), Sigma-Aldrich and used as received), and stirred using a magnetic stirrer. The

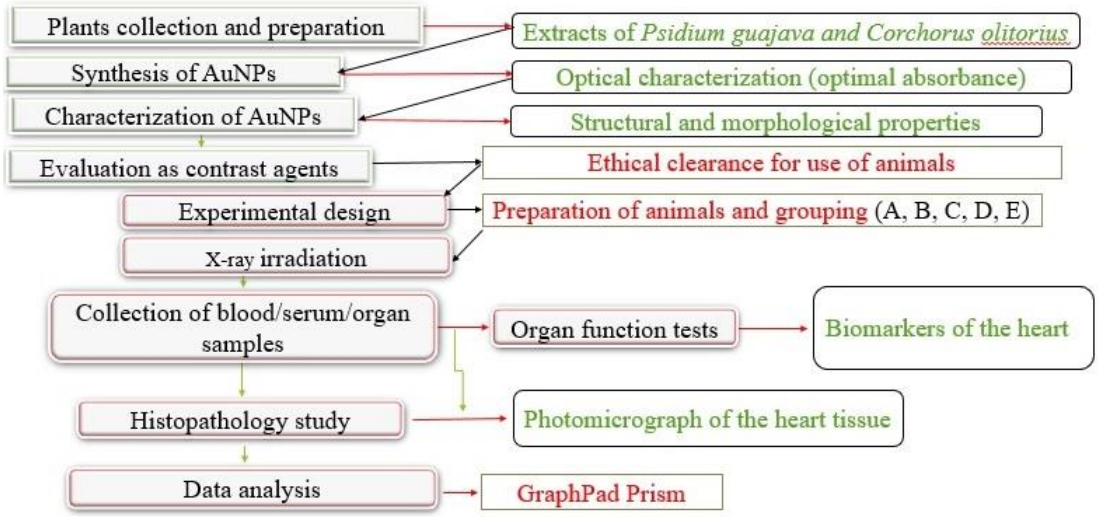

Fig. 1. The stepwise procedure used in conducting the experiment

color change was monitored before the reaction was further subjected to UV-Vis spectrophotometry analysis to investigate its absorbance. The reaction was modulated by further increasing the amount of the extract stepwise from 2 – 5 mL against that of the precursor (20 mL). The most optimized of each synthesized solution was thereafter subjected to other characterization.

Characterization

The prepared solutions were subjected to absorption spectroscopy using BIOBASE® UV-Vis spectrophotometer in the scanning range of 200 – 800 nm. The functional biomolecules was identified using Nicolet iS10 FTIR spectrometer at the range of 400 – 4000 cm^{-1}. The crystalline structure was determined using Rigaku MiniFlex Benchtop X-ray diffractometer operated at a voltage of 40 kV and current of 20 mA with a CuK∝ (λ = 1.54056 Å) radiation source. The elemental composition of the samples was undertaken under a scanning electron microscope JOEL JSM-7600F equipped with an energy-dispersive x-ray EDAX spectrometer operated at 15 kV. The morphology of the synthesized AuNPs was identified under JEOL JEM-2100 transmission electron microscopy (TEM), operated at 300 kV.

Animals

One hundred and fifty-six (156) male Wistar rats (270 ± 25 g) were used in this study. The animals were kept at room temperature of twelve hours (12 h) natural light-dark cycle and fed daily with animal pellet feed and water *ad libitum*. The rats were allowed to acclimatize. The Research Ethics Committee, Ministry of Health, Oyo State, Nigeria approved the experimental procedures and the animals received humane care in compliance with laid down guidelines as outlined in the guide for the care and use of laboratory animals [31].

Experimental Design

The rats were categorized into two: the first category is the unexposed and tagged group A. The rats in the second category were exposed and it consists of four (4) groups tagged: B, C, D and E. Group A served as the baseline control (BC) and consist of twelve (12) rats; the rats in this group were not administered any of the substances nor exposed to x-ray. Groups B, C, D, and E consist of twelve (12) rats in triplicate. The rats in group B serve as the experimental control (EC), as no substances were administered to the rats. The rats in group C were injected with the existing iodinated contrast agent (Urografin 76%, Berlimed S. A.) while those in groups D and E were administered the synthesized plant-based AuNPs from the extract of *Psidium guajava* and *Corchorus Olitorius* respectively. The substances were administered intraperitoneally at 6 mL/kg body weight of the rat [32 – 35].

X-ray irradiation

The rats in groups B, C, D and E were restrained inside an acrylic rectangular box and irradiated at the tube voltage of 40, 80 and 120 kV of x-ray respectively, at an exposure current 8 mAs with

the distance from source to the subject (rats) of 1 m using MARS Fixed X-ray, Allengers Medical Systems Ltd.

Collection of Samples

Six rats from each group/replicate were sacrificed on day 1 of the treatment and four weeks post-treatment (day 30) through cervical dislocation and samples of blood were collected via cardiac puncture. 3 mL of the blood was dispersed into lithium heparin tubes, allowed to clot for 45 min at room temperature, retracted and centrifuged at 3000 rpm for 15 minutes using a centrifuge to obtain serum. The heart was excised and divided into two equal halves. One portion of the tissue was immediately fixed in 10% formal saline to preserve the organ pending histopathology examination. The remaining half was washed in normal saline, homogenized on ice with 10 mM phosphate buffer (pH 7.4) at 5 ml of tissue weight, and thereafter centrifuged at 10,000 rpm to obtain supernatant. The serum and tissue supernatant was stored at -80°C pending analysis for the level of biomarkers activity.

Evaluation of Biomarkers activity

Samples of serum and tissue homogenate were retracted, and an aliquot of each sample was investigated for the markers of oxidative stress (superoxide dismutase (SOD), catalase (CAT), glutathione (GSH), malondialdehyde (MDA)); cardiac (creatine kinase (CK), troponin T (TnT), lactase dehydrogenase (LDH)) and inflammatory (interleukin-6 (IL-6), tumor necrosis factor-alpha (TNF- α) and caspase-3 (CAP3)). Each parameter was analyzed with appropriate commercially available kits following the protocols provided by the manufacturer.

Histopathology evaluation

Histopathological examination of the fixed heart tissue was undertaken to determine any abnormalities in the morphology of the heart and this was carried out following standard histopathology procedure.

Data Analysis

GraphPad Prism software (version 9.1.0 (221)) was used for the analysis of the data obtained. The results were presented as mean ± standard error of the mean (SEM). The data were also subjected to analysis of variance (ANOVA) with Dunnett's multiple comparisons post-hoc test at 0.001, 0.01, and 0.5 levels of significance.

RESULTS AND DISCUSSION

Absorbance spectra

The absorbance spectra revealed that there is a rapid decrease in the intensity of the AuNPs capped with *P. guajava* extract as the amount of the extract increases from 1 – 5 mL (Fig. 2a), while a gradual increase in the intensity of the *C. Olitorius* capped AuNPs (Fig. 2b) was obtained until a stable peak was reached at 3 mL before the intensity began to fall. 1 mL of *P. guajava* and 3 mL of *C. Olitorius* extract were found to be sufficient for the completion of bioreduction and therefore found to be the optimum for the formation of AuNPs. The surface plasmon resonance (SPR) peak of 534 nm and 538 nm was obtained for the AuNPs capped with the extract of *P. guajava* and *C. Olitorius* respectively, both of which fall within the characteristic range 510 – 560 nm of SPR band for AuNPs [36, 37].

Functional biomolecules

The spectra obtained for the biomolecules responsible for capping the AuNPs revealed the presence of different functional groups and their involvement in the formation of nanomaterials (Fig. 3). For the AuNPs capped with *P. guajava* (Fig. 3a), the peak observed at 3482 cm^{-1} could be assigned to stretching vibrations of –OH groups signifying the presence of alcohols, phenols, and flavonoids. The The peak is not in the spectrum; the peak at 1648 cm^{-1} is due to the C=O stretching of the carbonyl and carboxylic groups present in the amide linkage of the proteins, the peaks at 1508 could be assigned to the symmetrical stretch of carboxylate group; and the peaks at 1154 cm^{-1} is attributed to the C–O stretching of polyols, ether and alcoholic groups, and bending vibration of C–N. For the AuNPs capped with *C. Olitorius* (Fig. 3b), the major stretching appeared at 3000 – 3500 cm^{-1} and indicate the presence of -OH groups. The peaks at 2422 cm^{-1} indicate the presence of the amine linkage of protein and the peak at 1646 cm^{-1} was assigned to the C=O stretch. The C-C aromatics stretch was observed for both spectra at the region of 1416 cm^{-1}. Finally, C-O-C stretch can be found in the region of 1302 cm^{-1}. The peak at 1070 cm^{-1} could be assigned to the -OH vibrations of the proteins in the plants.

Crystalline structure

The diffractogram revealed a diffraction pattern of three (3) peaks at $2\theta = 38.45^{\circ}$ (111), 44.46° (200), and 64.75° for the AuNPs synthesized from *P. guajava*

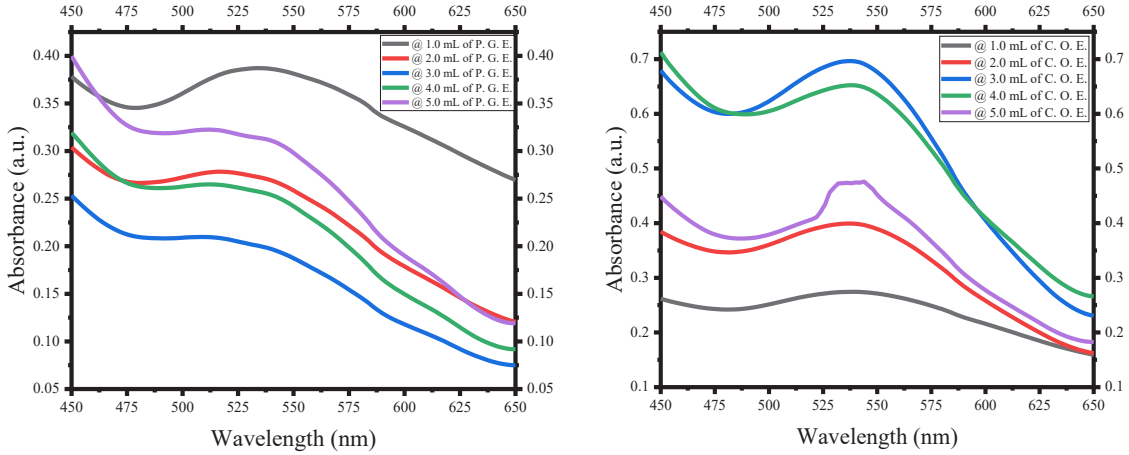

Fig. 2. Absorption spectra of AuNPs capped with (a) P. guajava (b) C. olitorius

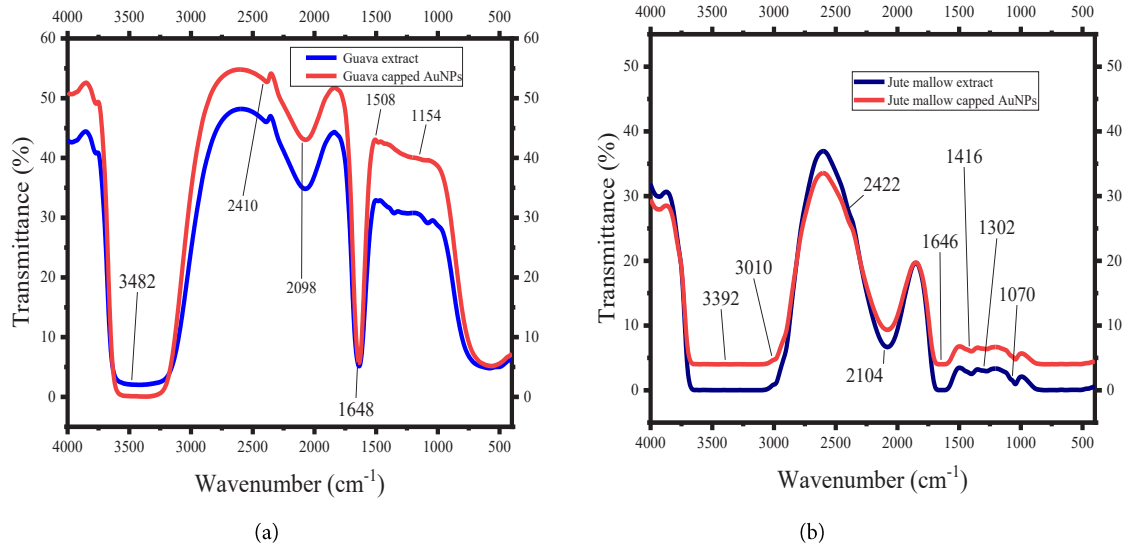

(a) (b)

Fig. 3. Functional biomolecules of AuNPs capped with (a) *P. guajava* (b) *C. Olitorius*

(Fig. 4a), while four (4) peaks at 2θ = 38.23˚ (111), 44.42˚ (200), 64.44˚ (220), and 77.39˚ (311) was obtained for the AuNPs synthesized from *C. Olitorius* (Fig. 4b). All the peaks revealed the structure of synthesized AuNPs to be face-centered cubic (FCC) structure of elemental gold as conformed with the standard database file of the Joint Committee on Powder Diffraction Standards (JCPDS, file number 00-004-0784). These peaks also conformed with the FCC structures of other green synthesized AuNPs reported in different studies [19, 38 – 42].

Elemental composition

Fig. 5 presents the EDX spectra obtained for the two different AuNPs. The spectra revealed the elemental composition of the synthesized AuNPs consisting of elemental gold (Au) which accounted for over 70% of the weight in both the analyzed samples. The spectra also revealed the presence of other elements such as C, O, Si, K, and Na, all of which may be associated with the elemental contents of the *P. guajava* (Fig. 5a) and *C. Olitorius* (Fig. 5b). Thus, the elemental composition obtained reflected the composition of the AuNPs. This elemental composition also aligned with the crystal structure obtained for the nanoparticle, both of which confirmed that AuNPs have been truly synthesized.

Morphological feature

Fig. 6 revealed the micrograph for the shape

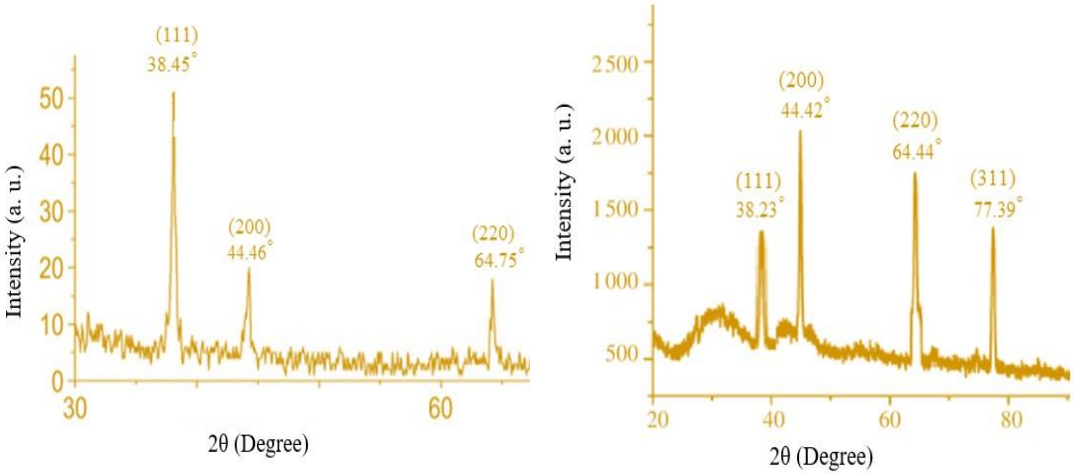

(a) (b)

Fig. 4. X-ray diffractogram of AuNPs capped with (a) *P. guajava* (b) *C. Olitorius*

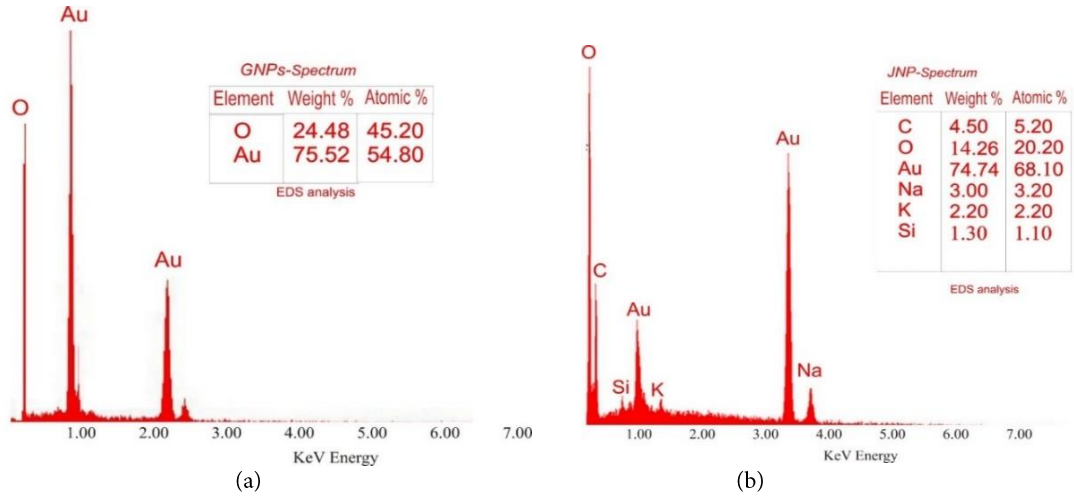

(a) (b)

Fig. 5. Elemental composition of AuNPs capped with extract of (a) P. guajava (b) C. Olitorius

and the histogram distribution of the particle size for the synthesized AuNPs capped with the extract of *P. guajava* and *C. Olitorius* respectively. The micrographs revealed the synthesized AuNPs are spherical in shape. The image analysis of the micrograph revealed the particle size to be in the range 5 – 11 nm with an average diameter of 8.23 ± 1.03 nm for the AuNPs capped *P. guajava* (Fig. 6a) and 3 – 10 nm with an average size of 6.57 ± 1.62 nm for the AuNPs capped *C. Olitorius* (Fig. 6b), both of which showed highly distributed nanoparticles.

Effect on biomarkers of heart

The results obtained for the biomarkers of the rat's heart on day 1 and 30 are presented in Tables 1 to 3 respectively. It was observed that at each of the x-ray tube voltage (40, 80 and 120 kV), there was a significant difference in the level of oxidative stress markers (Superoxide Dismutase (SOD), Catalase (CAT), Glutathione (GSH), Malonaldehyde (MDA)); cardiac markers (Creatine Kinase (CK), Lactate Dehydrogenase (LDH) and Troponin T (TnT)) as well as the inflammatory markers (Interleukin-6 (IL-6), Tumour Necrosis Factor-

Table 1a: Markers of the animal's heart injected and irradiated at 40 kV compared to the control on day 1

Indicators	A	B	C	D	E
SOD (µmol/g tissue)	8.24 ± 1.35	17.15 ± 3.90	6.66 ± 0.51[i]	10.94 ± 1.23	10.30 ± 3.23
CAT (µmol/g tissue)	1.78 ± 0.37	1.02 ± 0.22	1.13 ± 0.06	1.66 ± 0.15	1.57 ± 0.21
GSH (µmol/g tissue)	0.80 ± 0.12	0.89 ± 0.04	0.71 ± 0.09	0.86 ± 0.08	0.88 ± 0.07
MDA (µmol/g tissue)	24.64 ± 7.73	29.38 ± 6.96	17.35 ± 0.55	24.24 ± 8.16	24.88 ± 7.22
CK (U/L)	6.11 ± 0.73	13.69 ± 0.48[c]	7.64 ± 0.21[k]	6.44 ± 0.68	6.14 ± 1.72
LDH (U/L)	22.75 ± 0.65	23.63 ± 0.41	25.88 ± 0.01[b,i]	22.96 ± 0.33	23.69 ± 1.03
TnT (pg/ml)	2.62 ± 0.69	3.26 ± 0.23	7.13 ± 0.13[c,j]	2.72 ± 1.32	2.27 ± 0.22
IL-6 (pg/ml)	35.39 ± 9.44	28.41 ± 3.21	38.87 ± 1.55	36.12 ± 2.75	34.40 ± 3.57
TNF-α (pg/ml)	18.79 ± 1.91	50.14 ± 13.76	34.46 ± 5.83	18.84 ± 3.93	18.32 ± 1.17
CAP3 (ng/ml)	0.67 ± 0.12	0.77 ± 0.08	1.60 ± 0.05[c,k]	0.66 ± 0.22	0.70 ± 0.05

SOD – Superoxide Dismutase; CAT – Catalase; GSH – Glutathione; MDA – Malonaldehyde; TnT – Troponin T, CK - Creatine Kinase; LDH - Lactate Dehydrogenase; IL-6 – Interleukin-6; TNF-α - Tumour Necrosis Factor-alpha; CAP3 – Caspase 3

[a = i] significant at 0.05, [b = j] significant at 0.01, [c = k] significant at 0.001

a, b, c: statistically significant when compared to group A (control). i, j, k: statistically significant when compared to group B (x-ray only).

Table 1b: Markers of the animal's heart injected and irradiated at 40 kV compared to the control after day 30

Indicators	A	B	C	D	E
SOD (µmol/g tissue)	34.49 ± 5.52	23.76 ± 2.78	21.35 ± 2.08	34.28 ± 2.25	34.62 ± 2.56
CAT (µmol/g tissue)	5.00 ± 1.14	1.08 ± 0.16[c]	0.68 ± 0.05[c]	3.25 ± 0.01	3.79 ± 0.88
GSH (µmol/g tissue)	1.84 ± 0.26	1.53 ± 0.22	1.02 ± 0.17[a]	1.62 ± 0.14	1.78 ± 0.23
MDA (µmol/g tissue)	8.29 ± 1.16	14.31 ± 1.17	13.01 ± 1.85	7.38 ± 0.75	7.67 ± 1.12
CK (U/L)	9.63 ± 2.30	28.89 ± 5.54[a]	26.83 ± 6.46[a]	9.01 ± 2.30	9.38 ± 1.51
LDH (U/L)	33.89 ± 4.45	76.52 ± 8.56[a]	64.15 ± 18.12	34.39 ± 2.28	34.14 ± 3.13
TnT (pg/ml)	3.56 ± 0.60	4.99 ± 0.40	9.80 ± 0.65[c,k]	3.42 ± 0.95[i]	3.57 ± 0.80
IL-6 (pg/ml)	55.70 ± 5.76	92.51 ± 4.70	137.20 ± 17.63[c]	56.50 ± 8.25	54.23 ± 4.83
TNF-α (pg/ml)	44.51 ± 8.82	124.20 ± 1.32[b]	208.30 ± 0.66[c,j]	45.50 ± 33.13	43.29 ± 7.85
CAP3 (ng/ml)	0.77 ± 0.16	0.85 ± 0.05	1.29 ± 0.02[c,k]	0.82 ± 0.04	0.84 ± 0.60[b]

alpha (TNF-α); Caspase-3 (CAP3)) compared to those of the normal control (group A), experimental control (group B, x-ray only) and group C (Urografin) respectively.

Exposure of the heart to a foreign substance, whether toxic or not may produce oxygen-derived free radicals termed reactive oxygen species (ROS). These species namely hydroxyl radical (OH^-), superoxide radical anion (O^{2-}), and hydrogen peroxide (H_2O_2) cause severe damage to macromolecules, tissues, and organs through the process of lipid peroxidation, protein modification, and deoxyribonucleic acid (DNA) strand breaks [43, 44]. An imbalance between the production of ROS and the inability of the antioxidant systems to readily detoxify these reactive intermediates results in oxidative stress.

The importance of oxidative stress is commonly emphasized in the pathogenesis of various degenerative diseases, such as cardiovascular disorders or neurodegenerative diseases, diabetes, cancer [45 – 47]. Protective actions against ROS are performed by enzymes such as superoxide dismutase (SOD), catalase (CAT) and glutathione (GSH). Thus, whenever, the level of these antioxidants system decreases, the level of inactivated ROS rises, resulting in the ROS impairing the function of cardiac muscle cells, as it induced an energy deficit by affecting the function of proteins involved in energy metabolism and ultimately result in cardiac dysfunction and potential heart failure [48].

Lipid peroxidation is also a significant determinant of the degree of free radical generation, with MDA being one of the products and an important marker of the process of oxidative stress [49, 50]. Lipid peroxidation leads to the generation of free radicals which cause cell damage and lead to the release of marker enzymes. When the liver and kidney cell plasma membrane is damaged, a variety of enzymes normally located in the cytosol are released into the bloodstream. Thus, forcing the cardiac muscle to be significantly stressed.

Cardiac markers are endogenous substances released during circulation whenever the heart is damaged or stressed. The CK is mainly found in all muscle (cardiac and skeletal) and brain tissues. It plays an important role in energy storing mechanism of the tissues. Increased levels are found

Table 2a: Markers of the animal's heart injected and irradiated at 80 kV compared to the control on day 1

Indicators	A	B	C	D	E
SOD (µmol/g tissue)	8.24 ± 1.35	20.35 ± 3.21^{c}	7.94 ± 1.01^{j}	8.15 ± 1.03	8.35 ± 1.05
CAT (µmol/g tissue)	1.78 ± 0.37	0.83 ± 0.17^{a}	0.98 ± 0.07^{a}	1.58 ± 0.14	1.49 ± 0.16
GSH (µmol/g tissue)	0.80 ± 0.12	0.92 ± 0.03	0.73 ± 0.11	0.82 ± 0.07	0.81 ± 0.06
MDA (µmol/g tissue)	24.64 ± 7.73	40.09 ± 5.45	22.76 ± 2.82^{j}	22.89 ± 1.64	23.09 ± 2.74
CK (U/L)	6.11 ± 0.73	14.81 ± 0.61^{c}	10.28 ± 0.49^{b,j}	7.03 ± 1.35	7.53 ± 0.58^{i}
LDH (U/L)	22.75 ± 0.65	23.63 ± 0.00	26.93 ± 0.74^{c,j}	22.38 ± 0.63	22.14 ± 0.50
TnT (pg/ml)	2.62 ± 0.69	2.81 ± 0.02	8.35 ± 0.87^{c,k}	2.15 ± 0.81	2.23 ± 0.07
IL-6 (pg/ml)	35.39 ± 9.44	34.18 ± 4.25	64.84 ± 8.36	33.89 ± 6.21	35.02 ± 3.07
TNF-α (pg/ml)	18.79 ± 1.91	39.69 ± 6.35	112.80 ± 28.62^{c,i}	17.77 ± 1.23	18.07 ± 1.11
CAP3 (ng/ml)	0.67 ± 0.12	0.54 ± 0.04	1.45 ± 0.18^{b,j}	0.81 ± 0.27	0.82 ± 0.02

SOD – Superoxide Dismutase; CAT – Catalase; GSH – Glutathione; MDA – Malonaldehyde; TnT – Troponin T, CK - Creatine Kinase; LDH - Lactate Dehydrogenase; IL-6 – Interleukin-6; TNF-α - Tumour Necrosis Factor-alpha; CAP3 – Caspase 3$^{a=i}$ significant at 0.05, $^{b=j}$ significant at 0.01, $^{c=k}$ significant at 0.001

a, b, c: statistically significant when compared to group A (control). i, j, k: statistically significant when compared to group B (x-ray only).

Table 2b: Markers of the animal's heart injected and irradiated at 80 kV compared to the control after day 30

Indicators	A	B	C	D	E
SOD (µmol/g tissue)	34.49 ± 5.52	24.38 ± 5.12	25.44 ± 0.66	32.09 ± 2.23	32.99 ± 5.06
CAT (µmol/g tissue)	5.00 ± 1.14	2.01 ± 0.35^{b}	1.08 ± 0.21^{c,i}	4.35 ± 0.03^{k}	4.89 ± 0.10^{j}
GSH (µmol/g tissue)	1.84 ± 0.26	1.20 ± 0.23	1.07 ± 0.23	1.16 ± 0.16	1.07 ± 0.18
MDA (µmol/g tissue)	8.29 ± 1.16	14.68 ± 1.75	27.50 ± 3.26^{c,k}	7.89 ± 0.72^{i}	9.01 ± 1.31
CK (U/L)	33.89 ± 4.45	36.01 ± 1.01^{a}	63.02 ± 7.81^{c,j}	34.32 ± 5.36	36.01 ± 2.03^{a}
LDH (U/L)	9.63 ± 2.30	20.64 ± 1.85^{a}	16.51 ± 1.51	10.27 ± 4.84^{i}	9.88 ± 2.30^{j}
TnT (pg/ml)	3.56 ± 0.60	3.93 ± 0.54	9.46 ± 0.97^{c,k}	4.03 ± 0.61	3.97 ± 0.65
IL-6 (pg/ml)	44.51 ± 8.82	68.11 ± 5.28	160.60 ± 12.85^{c,j}	46.04 ± 2.39	45.58 ± 3.69
TNF-α (pg/ml)	55.70 ± 5.76	87.25 ± 4.70	236.20 ± 32.20^{c,k}	58.64 ± 8.18	56.54 ± 5.14
CAP3 (ng/ml)	0.77 ± 0.16	0.73 ± 0.03	1.40 ± 0.19^{c,k}	0.87 ± 0.07	0.80 ± 0.02

in myocardial infarction (MI), muscular dystrophy, cerebrovascular-disease, pulmonary infarction, electrical shocks and hypothyrodisim. The LDH enzyme is found in all organ cells, but especially in cardiac and skeletal muscle, liver, kidney and red blood cells (RBCs). Elevated levels are also found in MI, liver diseases, hemolytic anaemias, pernicious anaemia, leukemia and pulmonary diseases.

Troponin is the most sensitive and specific test for myocardial damage because it has increased specificity compared with CK and LDH. Troponin is released during MI from the cytosolic pool of the myocytes and its release is prolonged with the degradation of actin and myosin filaments. The differential diagnosis of TnT elevation includes acute infarction, severe pulmonary embolism causing acute right heart overload, heart failure, and myocarditis [51]. Inflammation is a normal biological response of the body to physical or chemical agents, tissue damage, and infections in which the production of inflammatory mediators such as cytokines, and ROS is triggered. If not controlled, these inflammatory mediators are over-produced which can induce pathological processes linked to several chronic conditions [52].

Photomicrograph of the organs

The photomicrograph of the rat's heart tissue sections stained by hematoxylin and eosin (H & E) are shown in Fig. 7. The cellular structures of the heart showed a normal epicardial layer, with the myocardial layer showing a focal area of mild degeneration and inflammatory cells in Group A and moderate congestion in Group B compared to those of groups C, D and E. All the groups had normal myocytes. The photomicrograph of group C revealed moderately infarcted myocytes in the myocardial layer while those of Groups D and E revealed normal epicardial layer, myocardial layer and myocytes.

Thus, it was observed that the antioxidant defense mechanisms of the rats in group C is low while those of groups D and E is high compared to those of group A (baseline control). Likewise,

Table 3a: Markers of the animal's heart injected and irradiated at 120 kV compared to the control on day 1

Indicators	A	B	C	D	E
SOD (µmol/g tissue)	8.24 ± 1.35	10.79 ± 0.45	8.01 ± 0.40	8.13 ± 1.41	9.20 ± 0.74
CAT (µmol/g tissue)	1.78 ± 0.37	1.08 ± 0.16	0.67 ± 0.05^{b}	1.46 ± 0.17^{b}	0.81 ± 0.13^{b}
GSH (µmol/g tissue)	0.80 ± 0.12	0.94 ± 0.06	0.97 ± 0.09	0.81 ± 0.05	0.90 ± 0.06
MDA (µmol/g tissue)	24.64 ± 7.73	17.01 ± 1.18	21.37 ± 2.92	18.77 ± 1.86	20.00 ± 2.11
CK (U/L)	6.11 ± 0.73	22.27 ± 3.48^{a}	17.41 ± 1.83	6.29 ± 1.27	14.58 ± 0.62
LDH (U/L)	22.75 ± 0.65	24.57 ± 0.19	27.45 ± 0.81^{c,j}	22.61 ± 0.01	24.20 ± 0.75
TnT (pg/ml)	2.62 ± 0.69	2.96 ± 0.03	8.96 ± 0.94^{c,k}	3.23 ± 0.15	3.35 ± 0.28
IL-6 (pg/ml)	35.39 ± 9.44	32.98 ± 0.24	77.82 ± 1.94^{c,k}	34.80 ± 1.65	34.90 ± 7.42
TNF-α (pg/ml)	18.79 ± 1.91	22.27 ± 3.48	52.00 ± 17.52^{c,k}	19.12 ± 21.68	18.65 ± 2.18
CAP3 (ng/ml)	0.67 ± 0.12	0.92 ± 0.08	1.37 ± 0.21^{b}	0.76 ± 0.19	0.79 ± 0.03

SOD – Superoxide Dismutase; CAT – Catalase; GSH – Glutathione; MDA – Malonaldehyde; TnT – Troponin T, CK - Creatine Kinase; LDH - Lactate Dehydrogenase; IL-6 – Interleukin-6; TNF-α - Tumour Necrosis Factor-alpha; CAP3 – Caspase 3

$^{a=i}$ significant at 0.05, $^{b=j}$ significant at 0.01, $^{c=k}$ significant at 0.001

a, b, c: statistically significant when compared to group A (control). i, j, k: statistically significant when compared to group B (x-ray only).

Table 3b: Markers of the animal's heart injected and irradiated at 120 kV compared to the control after day 30

Indicators	A	B	C	D	E
SOD (µmol/g tissue)	34.49 ± 5.52	30.68 ± 1.23	22.41 ± 4.87	34.70 ± 3.35	32.05 ± 4.96
CAT (µmol/g tissue)	5.00 ± 1.14	2.82 ± 0.69	1.07 ± 0.21^{c,i}	4.48 ± 0.02	4.54 ± 0.20^{k}
GSH (µmol/g tissue)	1.84 ± 0.26	1.26 ± 0.29	0.93 ± 0.14^{a}	1.32 ± 0.23	1.51 ± 0.06
MDA (µmol/g tissue)	8.29 ± 1.16	16.35 ± 0.58^{c}	15.82 ± 0.93^{c}	8.65 ± 1.47^{j}	8.20 ± 0.81^{j}
CK (U/L)	33.89 ± 4.45	47.83 ± 10.56	46.51 ± 9.52	34.27 ± 2.03^{j}	33.59 ± 3.19
LDH (U/L)	9.63 ± 2.30	19.95 ± 2.24	26.14 ± 7.73^{a}	8.92 ± 0.51	9.76 ± 0.74
TnT (pg/ml)	3.56 ± 0.60	3.94 ± 0.55	5.09 ± 0.14^{a}	3.24 ± 0.27^{j}	3.52 ± 0.17^{k}
IL-6 (pg/ml)	44.51 ± 8.82	87.79 ± 12.16	85.20 ± 13.30^{b}	42.89 ± 3.01^{j}	43.90 ± 4.92
TNF-α (pg/ml)	55.70 ± 5.76	82.87 ± 9.54	85.40 ± 47.19^{a}	53.10 ± 6.39^{j}	55.60 ± 4.75^{b}
CAP3 (ng/ml)	0.77 ± 0.16	0.80 ± 0.03	1.10 ± 0.07^{i}	0.80 ± 0.08	0.79 ± 0.08

it was also observed that the SOD and MDA level of the rats in group B (experimental control) has the highest value. Similar pattern was observed in the cardiac and inflammatory markers of the rats injected with the synthesized AuNPs compared to those of groups B and C. This is an indication that x-ray induces stress on the myocardium by producing more ROS an action that may lead to myocardial ischemia or infarction. However, the administered substances reduce the stress by producing antioxidants to detoxify the free radicals with the rats administered with the plant-based AuNPs producing more antioxidants compared to those administered with the iodinated CA (Urografin).

Thus, with the higher atomic number and absorption coefficient of gold (Au) compared to those of iodine (I), Au provides about 2.7 times greater contrast per unit weight than I, and to which there was no evidence of toxicity at 6 mL/kg body weight of the rat on the cardiac cells. The rats injected with the plant-based AuNPs showed positive significant antioxidant, cardiac and inflammatory effects than those injected with the iodinated CA (Urografin) by protecting the heart. Hence, it can be inferred that the cardioprotective role of biosynthesized AuNPs may be attributed to the abundance of antioxidants present in the leaves of *P. guajava* and *C. Olitorius* [53]. The findings in this study conformed with the report of Vinodhini *et al* reporting the cardioprotective potential of biobased AuNPs from proanthocyanidin [21] and Mehanna *et al* reporting a significant decrease in antioxidant and inflammatory indicators when investigating the effects of AuNPs shape and dose on immunological, hematological, inflammatory, and antioxidants parameters in male rabbits [54]. The present study also confirms the hypothesis that the biomedical applications of AuNPs vary according to the stabilizing molecule.

CONCLUSION

Thus, while several studies are proposing the utilization of AuNPs as a novel CA for x-ray imaging, the findings in this study demonstrated that biosynthesized AuNPs will be useful as CAs

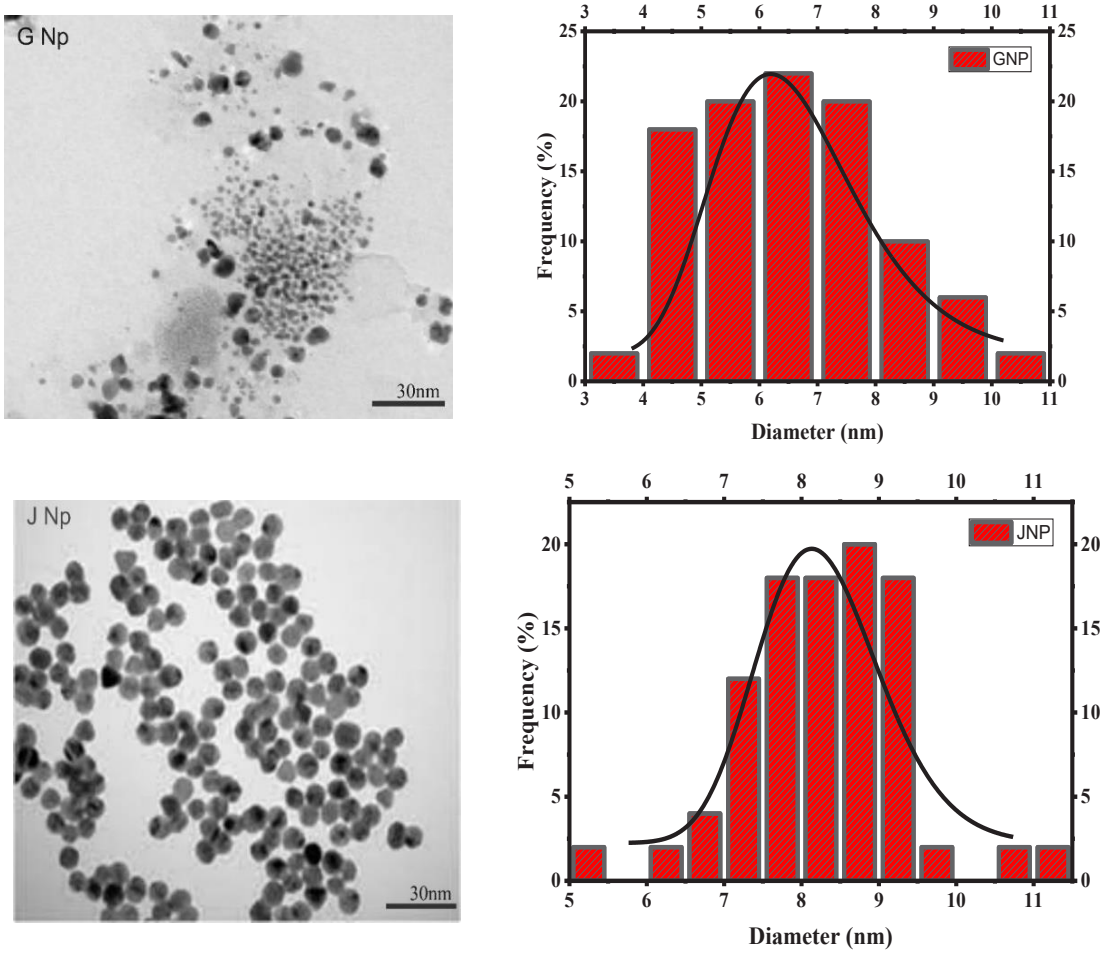

Fig. 6. Micrograph and size distribution of AuNPs capped extract of (a) *P. guajava* (b) *C. olitorious*

and offer significant advantages over the existing iodinated CA without affecting the hemodynamics of the cardiovascular system. The single-step green process has proven to be effective for the synthesis and stabilization of biocompatible AuNPs as the phytochemicals and antioxidants present in the assayed plants protect the cardiac cells from all forms of cardiovascular injury. Hence, the incorporation of nanotechnology into medicine will be helpful in the development of new drugs for various biomedical applications. The findings in this study serve as a yardstick for further studies and will also aid in the use of biosynthesized AuNPs for several biomedical applications.

CREDIT AUTHORSHIP CONTRIBUTION STATEMENT

Conceptualization and study design: APS, IGA, AMK.
Methodology: APS, IGA, SWA, AMK, SYK
Data analysis: APS, IGA, SWA, AO, AAG.
Visualization: APS, IGA, SWA, LMK and AAG.
Supervision: IGA, AMK, and SWA.
Funding acquisition: APS, IGA.
Intellectual input: APS, IGA, SWA, SYK, AO, AAG.
Project administration: IGA, SWA, AMK, AO
Writing (original draft): APS, IGA, SWA
Writing (review and editing): All authors.

ACKNOWLEDGMENTS

The authors appreciate the Radiographer and Technical Staff at the Radiography Unit of Ladoke Akintola University of Technology Health Centre for their vital contributions towards the actualization of the research.

CONFLICT OF INTEREST

The authors declare no conflict of interest.

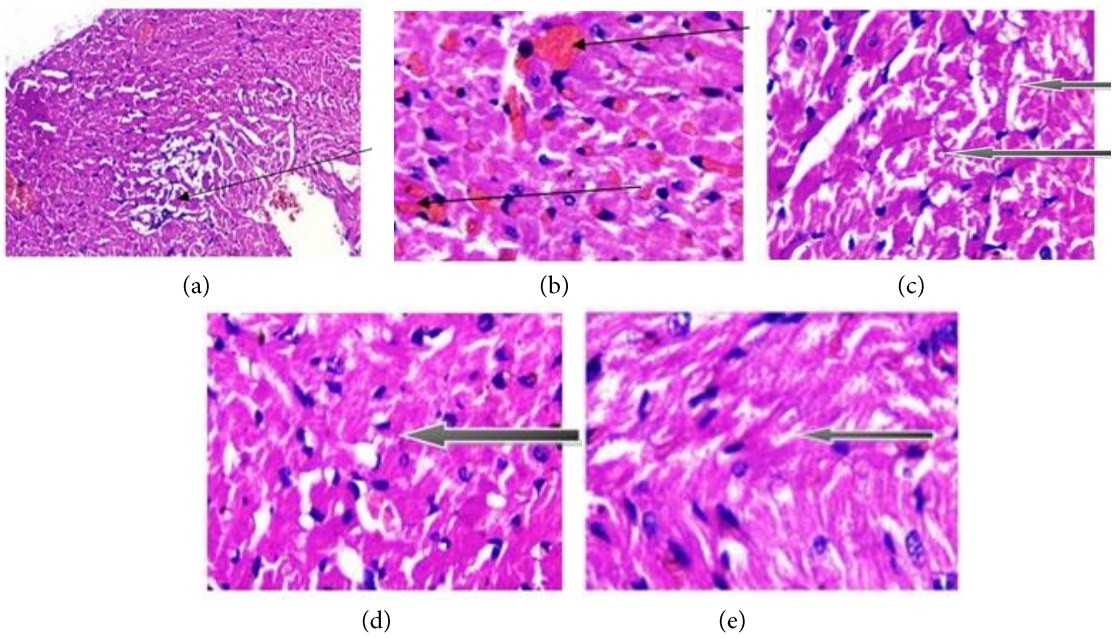

Fig. 7: Photomicrograph of the heart sections of the rats stained by Haematoxylin and Eosin (a) group A showed normal epicardial layer, the myocardial layer show focal area of mild degeneration and inflammatory cells (slender arrow) with normal myocytes (b) group B showed normal epicardial layer and the myocardial layer appear normal, the myocytes are normal with moderate congestion (slender arrow) (c) group C showed normal epicardial layer, the myocardial layer show moderately infarcted myocytes (black arrow) (d) group D showed normal epicardial layer, the myocardial layer and myocytes appear normal (e) group E showed normal epicardial layer and the myocardial layer and myocytes appear normal (black arrow).

FUNDING

This research did not receive any specific grant from funding agencies in the public, commercial, or not-for-profit sectors.

REFERENCES

1. Suetens P. Fundamentals of medical imaging. Cambridge university press; 2017 May 11. https://doi.org/10.1017/9781316671849
2. Bushberg JT, Seibert JA, Leidholdt EM, Boone JM. The essential physics of medical imaging. 3rd ed. Philadelphia: Lippincott Williams & Wikings; 2012.
3. Cormode DP, Skajaa T, Fayad ZA, Mulder WJM. Nanotechnology in medical imaging: Probe design and applications. Arterioscler Thromb Vasc Biol, 2009; 29(7): 992-1000. https://doi.org/10.1161/ATVBAHA.108.165506
4. Armanmehr M, Jalali M, Shokri A, Heydari Chaleshtori A. The Effect of Cobalt Oxide Nanoparticles on Improving the Quality of Computerized Tomography (CT) Scan Medical Imaging. Iran J Med Phys 2022; 19: 154-158. 10.22038/IJMP.2021.59219.1996.
5. Cho EC, Glaus C, Chen J, Welch MJ, and Xia Y. Inorganic Nanoparticle-Based Contrast Agents for Molecular Imaging. Trends Mol. Med., 2010; 16(12): 561-573 https://doi.org/10.1016/j.molmed.2010.09.004
6. Bae KT. Intravenous Contrast Medium Administration and Scan Timing at CT: Considerations and Approaches 1. Radiology; 2010; 256(1):32 - 61. https://doi.org/10.1148/radiol.10090908
7. Suchal K, Malik S, Gamad N, Malhotra RK, Goyal SN, Bhatia J, Arya DS. Kampeferol protects against oxidative stress and apoptotic damage in experimental model of isoproterenol-induced cardiac toxicity in rats. Phytomed. Int. J. Phys. Phytopharmacol. 2016, 23, 1401-1408. https://doi.org/10.1016/j.phymed.2016.07.015
8. Verma VK, Malik S, Narayanan SP, Mutneja E, Sahu AK, Bhatia J, Arya DS. Role of MAPK/NF-kappaB pathway in cardioprotective of Morin in isoproterenol induced myocardial injury in rats. Mol. Biol. Rep. 2019, 46, 1139-1148. https://doi.org/10.1007/s11033-018-04575-9
9. Wang H, Naghavi M, Allen C, Barber RM, Bhutta ZA, Carter A, et al. (GBD 2015 Mortality and Causes of Death Collaborators) (October 2016). "Global, regional, and national life expectancy, all-cause mortality, and cause-specific mortality for 249 causes of death, 1980-2015: a systematic analysis for the Global Burden of Disease Study 2015". Lancet. 388 (10053): 1459-1544. doi:10.1016/S0140-6736(16)31012-1 https://doi.org/10.1016/S0140-6736(16)31012-1
10. Ahn S, Jung YS, and Lee SJ. Gold Nanoparticle Contrast Agents in Advanced X-ray Imaging Technologies, Molecules, 2013; 18, 5858 - 5890 https://doi.org/10.3390/molecules18055858
11. De La Vega JC, and Häfeli UO. Utilization of nanoparticles as X-ray contrast agents for diagnostic imaging applications, Contrast Media Mol. Imaging, 2015; 10: 81-95 https://doi.org/10.1002/cmmi.1613
12. Hainfeld JF, Slatkin DN, Focella TM, Smilowitz HM. Gold nanoparticles: A new X-ray contrast

agent. Br J Radiol, 2006; 79(939): 248-253. https://doi.org/10.1259/bjr/13169882
13. Seltzer SE, Blau M, Herman LW, Hooshmand RL, Herman LA, Adams DF, Minchey SR, Janoff AS. Contrast material-carrying liposomes: biodistribution, clearance, and imaging characteristics. Radiology, 1995; 194 (3), 775- 781. https://doi.org/10.1148/radiology.194.3.7862978
14. Jadoun S, Arif R, Jangid NK, Meena RK. Green synthesis of nanoparticles using plant extracts: A review. Environ Chem Lett, 2021; 19:355e74. https://doi.org/10.1007/s10311-020-01074-x. https://doi.org/10.1007/s10311-020-01074-x
15. Jha AK, Prasad K, Kulkarni AR.(2009): Plant system: Nature's nanofactory. Colloids and Surfurces B: Biointerfaces, 73(2): 219-223. https://doi.org/10.1016/j.colsurfb.2009.05.018
16. Thakkar KN, Mhatre SS, Parikh RY. Biological synthesis of metallic nanoparticles. Nanomedicine: Nanotechnology, Biology and Medice; 2010; 6(2): 257-262. https://doi.org/10.1016/j.nano.2009.07.002
17. Yasmin A, Ramesh K, and Rajeshkumar S. Optimization and stabilization of gold nanoparticles by using herbal plant extract with microwave heating. Nano Convergence,, 2014; 1(12): 1- 7. https://doi.org/10.1186/s40580-014-0012-8
18. Kumar M., Tomar M., Amarowicz R., Saurabh V., Nair M. S., Maheshwari C., Sasi M., Prajapati U., Hasan M., Singh, S., Changan S., Prajapat R. K., Berwal M. K., Satankar V. Guava (Psidium guajava L.) Leaves: Nutritional Composition, Phytochemical Profile, and Health-Promoting Bioactivities. Foods, 2021; 10, 752. https://doi.org/10.3390/foods10040752
19. Ismail EH, Saqer AMA, Assirey E, Naqvi A, Okasha RM. Successful Green Synthesis of Gold Nanoparticles using a Corchorus olitorius Extract and their Antiproliferative Effect in Cancer Cells. Int. J. Mol. Sci., 2018; 19, 2612: 1-14. https://doi.org/10.3390/ijms19092612
20. Yokoyama S, Hirimoto K, Fuikawa T, Kondo H, Konishi N, Sudo S, Iwashima M, Ooi K. Topical application of Corchorous olitorus leaf extract ameliorates atopic dermatitis in NC/Nga mice. Dermatol. Asp., 2014, 2; 3 - 10. https://doi.org/10.7243/2053-5309-2-3
21. Vinodhini A, Govindarajuc K, Singaravelua G, Sadiq MA, Kumar GV. Cardioprotective potential of biobased gold nanoparticles. Colloids and Surfaces B: Biointerfaces, 2014, 117; 480-486 https://doi.org/10.1016/j.colsurfb.2014.01.006
22. Soni N, and Prakash S. Green nanoparticles for mosquito control. Sci World J.; 2014:1. https://doi.org/10.1155/2014/496362
23. Rahul S, Chandrashekhar P, Hemant B, Bipinchandra S, Mouray E, Grellier P, Satish P. In vitro antiparasitic activity of microbial pigments and their combination with phytosynthesized metal nanoparticles. Parasitol Int.; 2015, 64:353-356. https://doi.org/10.1016/j.parint.2015.05.004
24. Lakshmana A, Umamaheswari C, Nagarajan NS. A facile phytomediated synthesis of gold nanoparticles using aqueous extract of Momordica cochinchinensis rhizome and their biological activities. J Nanosci Technol., 2016, 2:76-80.
25. Vijayan R, Joseph S, Mathew B. Eco-friendly synthesis of silver and gold nanoparticles with enhanced antimicrobial, antioxidant, and catalytic activities. IET Nanobiotechnol.; 2018, 12:850-856. https://doi.org/10.1049/iet-nbt.2017.0311
26. Patil MP, and Kim GD. Eco-friendly approach for nanoparticles synthesis and mechanism behind antibacterial activity of silver and anticancer activity of gold nanoparticles. Appl Microbiol Biotechnol, 2017, 101:79-92. https://doi.org/10.1007/s00253-016-8012-8
27. Patil MP, Ngabire D, Thi HHP, Kim MD, Kim GD. Eco-friendly synthesis of gold nanoparticles and evaluation of their cytotoxic activity on cancer cells. J Clust Sci.; 2017, 28:119-132. https://doi.org/10.1007/s10876-016-1051-6
28. Zadeh A, Shahhosseini F, Rasoolzadegan E., Özbolat GS and Farahbod, F.. Au nanoparticles in the diagnosis and treatment of ovarian cancer: A new horizon in the personalized medicine. Nanomedicine Research Journal, 2022, 7(1), 1-18. doi: 10.22034/nmrj.2022.01.001
29. Akbari A, Eshkiki SZ, Mayahi S, and Amini SM. In-vitro investigation of curcumin coated gold nanoparticles effect on human colorectal adenocarcinoma cell line. Nanomedicine Research Journal, 2022, 7(1), 66-72. doi: 10.22034/nmrj.2022.01.006
30. Rad MR, Kazemian H, Yazdani F, Monfared MRZ, Rahdar H, Javadi A, Kodori M. Antibacterial activity of gold nanoparticles conjugated by aminoglycosides against A. baumannii isolates from burn patients. Recent Pat Anti-infect Drug Discov., 2018, 13(3):256-264. https://doi.org/10.2174/1574891X13666180828115543
31. National Research Council. Guide for the Care and Use of Laboratory Animals. Washington, DC: The National Academies Press, 2011
32. Turner PV, Brabb T, Pekow C, & Vasbinder MA. Administration of substances to laboratory animals: routes of administration and factors to consider. Journal of the American Association for Laboratory Animal Science: JAALAS, 2011; 50(5), 600-613.
33. Abdelhalim MA, and Abdelmottaleb MSA. The gold nanoparticle size and exposure duration effect on the liver and kidney function of rats: In vivo. Saudi journal of biological sciences, 2013; 20(2), 177-181. https://doi.org/10.1016/j.sjbs.2013.01.007
34. Al-Neami AQ, Al-Karam LQ, Humadi MD, and Alwan MH. Applications and Advantages of Gold Nanoparticles as X-Ray Contrast Agent. J Biomed Eng Med Devic, 2017; 2(2): 1-3 https://doi.org/10.4172/2475-7586.1000128
35. Pandy V. A simple method for animal dose calculation in preclinical research, EC
Pharmacology and Toxicology, 2020; 8(3):1 - 2.
36. Sujitha MV, Kannan S. Green Synthesis of Gold Nanoparticles Using Citrus Fruits (Citrus limon, Citrus reticulata and Citrus sinensis) Aqueous Extract and Its Characterization. Spectrochimica Acta Part A: Molecular and Biomolecular Spectroscopy, 2013; 102: 15-23. http://dx.doi.org/10.1016/j.saa.2012.09.042 https://doi.org/10.1016/j.saa.2012.09.042
37. Geraldes AN, da Silva AA, Leal J, Estrada-Villegas GM, Lincopan N, Katti KV, Lugão AB. Green Nanotechnology from Plant Extracts: Synthesis and Characterization of Gold Nanoparticles. Advances in Nanoparticles, 2016; 5, 176-185. http://dx.doi.org/10.4236/anp.2016.53019 https://doi.org/10.4236/anp.2016.53019
38. Aljabali AAA, Akkam Y, Al Zoubi MS, Al-Batayneh KM, Al-Trad B, Alrob AO, Alkilany AM, Benamara M, Evans

DJ. Synthesis of Gold Nanoparticles Using Leaf Extract of Ziziphus zizyphus and their Antimicrobial Activity. Nanomaterials,2018;8(174):1-15;doi:10.3390/nano8030174 https://doi.org/10.3390/nano8030174

39. Karuppiah C, Palanisamy S, Chen SM, Emmanuel R, Muthupandi K, Prakash P. Green synthesis of gold nanoparticles and its application for the trace level determinationofpainter'scolic.RSCAdv.2015,5,16284-16291 https://doi.org/10.1039/C4RA14988B
40. Dwivedi AD, Gopal K. Biosynthesis of silver and gold nanoparticles using chenopoduim album leaf extract. Colloids Surf. A Physicochem Eng. Aspects, 2010; 369, 27-33 https://doi.org/10.1016/j.colsurfa.2010.07.020
41. Dubey SP, Lahtinen M, Sillanpaa M. Tanasy fruit mediated green synthesis of silver and gold nanoparticles. Process Biochem. 2010; 45, 1065-1071 https://doi.org/10.1016/j.procbio.2010.03.024
42. Das S, Roy P, Mondal S, Bera T, Mukherjee A. One pot synthesis of gold nanoparticles and application in chemotherapy of wild and resistant type of visceral leishmaniasis Colloids Surf. B Biointerfaces, 2013; 107, 27-34 https://doi.org/10.1016/j.colsurfb.2013.01.061
43. Sun AY, and Chen YM. Oxidative stress and neurodegenerative disorders. J. Biomed. Sci, 1998; 5: 401 - 414 https://doi.org/10.1007/BF02255928
44. Zaidi SM, and Banu N. Antioxidant potential of vitamins A, E and C in modulating oxidative stress in rats brain. Clin. Chim. Acta, 2004; 340: 229 - 33 https://doi.org/10.1016/j.cccn.2003.11.003
45. Halliwell B and Gutteridge JMC. Oxidative stress: adaptation, damage, repair and death. In editors. Free radicals in biology and medicine. Oxford, UK: Oxford University Press, 1999; 284 - 330
46. Abuja PM. and Albertini R. Methods for monitoring oxidative stress, lipid peroxidation and oxidative resistance of lipoproteins. Clinica Chimica Acta, 2001; 306: 1 - 7 https://doi.org/10.1016/S0009-8981(01)00393-X
47. Apostolova N, Blas-Garcia A, Esplugues JV. Mitochondria sentencing about cellular life and death: a matter of oxidative stress. Curr Pharm Des., 2011; 17: 4047-60. https://doi.org/10.2174/138161211798764924
48. van der Pol A, van Gilst WH, Voors AA, van der Meer P. Treating oxidative stress in heart failure: past, present and future. Eur J Heart Fail, 2019; 21(4):425-435. https://doi.org/10.1002/ejhf.1320
49. Halliwell B and Gutteridge JMC. Lipid peroxidation oxygen radicals, cell damage and antioxidant theraphy. Lancet, 1994;1: 1396 - 1397. https://doi.org/10.1016/S0140-6736(84)91886-5
50. Chaudiere J and Ferrari-Iliou R. Intracellular antioxidants: from chemical to biochemical mechanisms. Food Chem Toxicol, 1999; 37: 949 - 962. https://doi.org/10.1016/S0278-6915(99)00090-3
51. Dasgupta A and Wahed A. Clinical Chemistry, Immunology and Laboratory Quality Control (Second Edition), 2021; 149-171, Elsevier. https://doi.org/10.1016/B978-0-12-815960-6.00008-X
52. Leyva-López N, Gutiérrez-Grijalva EP, Vazquez-Olivo G, Heredia JB. Essential Oils of Oregano: Biological Activity beyond Their Antimicrobial Properties. Molecules, 2017; 22(6):989. https://doi.org/10.3390/molecules22060989
53. Suchal K, Malik S, Gamad N, Malhotra RK, Goyal SN, Bhatia J, Arya DS. Kampeferol protects against oxidative stress and apoptotic damage in experimental model of isoproterenol-induced cardiac toxicity in rats. Phytomed. Int. J. Phys. Phytopharmacol. 2016, 23: 1401-1408. https://doi.org/10.1016/j.phymed.2016.07.015
54. Mehanna ET, Kamel BSA, Abo-Elmatty DM, Elnabtity SM, Mahmoud MB, Abdelhafeez MM, Abdoon ASS (2022): Effect of gold nanoparticles shape and dose on immunological, hematological, inflammatory, and antioxidants parameters in male rabbit, Veterinary World, 15(1): 65-75. https://doi.org/10.14202/vetworld.2022.65-75